The (010) surface of the Al45Cr7 complex intermetallic compound : insights from Density Functional Theory

Florian Brix, Romain Simon, Émilie Gaudry

The (010) surface of the $Al_{45}Cr_7$ complex intermetallic compound : insights from Density Functional Theory

F. Brix[a], R. Simon[a,b], É. Gaudry*[a,b]

Dedicated to Professor Juri Grin on the Occasion of his 65th Birthday

* Prof. Émilie Gaudry
Email: Emilie.Gaurdy@univ-lorraine.fr
[a] Univ. Lorraine, CNRS, Institut Jean Lamour, F-54000 Nancy, France
[b] École des Mines de Nancy, Univ. L F-54000 Nancy, France

Abstract: The $Al_{45}Cr_7$ compound is considered to exhibit an approximant structure of the icosahedral Al_4Cr phase. Its (010) surface has been investigated in detail using density functional calculations. Surface energy calculations show that the stable terminations {result} from a cleavage of the crystal between adjacent atomic planes, in agreement with the layered structure of the compound. The integrity of the icosahedral atomic arrangements (icosahedral clusters) found in the bulk structure, is predicted to be removed at the surface. This result is in contrast to what has been previously concluded for the (010) surface of the $Al_{13}Fe_4$ quasicrystal approximant. Our findings are discussed in relation to the bonding network in the compound, calculated using the Crystal Orbital Hamiltonian Population approach, as possible reasons for such contrasted behavior.

Introduction

Intermetallics belong to a class of inorganic compounds which is considered to be one of the most complex, both by the diversity of its crystal structures and by the large number of atoms contained in the corresponding crystal cells. More than 900 structure types are identified among binary compounds [1], and giant cells that contain hundreds and thousands of atoms have been recently identified in a few ternaries [2,3,4]. Such complex structures originate from the ability of the constituent atoms to adopt a range of coordination numbers and a variety of coordination environments, thus leading to a description of bulk structures as stacking of highly symmetric atomic polyhedra. Intensive studies of the chemical and physical properties of intermetallic compounds have led to many suggestions for potential applications [5], such as thermoelectric, magnetic, corrosion resistant and hydrogen storage materials, etc. Applications involving intermetallics surfaces, like coatings and heterogeneous catalysts, are maybe the most promising [6,7,8]. However, while the surface structures of simple metals and alloys have been extensively studied these last years, surfaces of complex intermetallic compounds still represent a largely unexplored field.

In the case of simple metals or alloys, a surface model would typically be a flat plane, with atomic steps separating terraces, if deep restructuring phenomena like reconstruction, segregation or roughening are excluded [9,10]. It is also what is observed with Al-based quasicrystals prepared under ultra-high vacuum by cycles of sputtering and annealing : terminations form at specific bulk planes, i.e. dense planes with a high content of the lowest surface energy element presenting large interlayer spacing in the bulk [11,12,13]. However, when dealing with complex intermetallic compound surfaces, more corrugated surface structures may arise, as already observed in a few cases [14,15,16,17], in the form of highly cohesive clusters emerging from the bulk lattice.

In this paper, we focus on the (010) surface of the $Al_{45}Cr_7$ compound, considered to exhibit an *approximant* structure of the icosahedral i-Al_4Cr phase. The bulk structure, first determined by Cooper (mC104, *C2/m*) [18], is characterized by icosahedrally coordinated Cr. Like other intermetallics in the Al-rich part of the Al-Cr phase diagram [19,20] – η-$Al_{11}Cr_2$ [21] and several polymorphs of Al_4Cr (μ-Al_4Cr [22], ε-Al_4Cr [23]) – this compound presents characteristic features of pseudo-icosahedral symmetry. The investigation of $Al_{45}Cr_7$(010) will then contribute to extend our knowledge on cluster-based inter-metallic surfaces.

Another motivation for this work comes from metallurgy. Chromium is well-known as a grain refiner in the aluminum foundry industry [24], and recent experiments suggest that the formation of the face-centered cubic Aluminum phase in the under-cooled liquid occurs on icosahedron quasicrystals or related phases, like the parent stable $Al_{45}Cr_7$ phase [25,26]. Recent surface science experiments performed under ultra-high vacuum support the formation of an fcc Al film with (111) orientation on $Al_{45}Cr_7$(010), while suggesting a nano-structured surface morphology for the substrate [27]. However, no surface model has been proposed so far for $Al_{45}Cr_7$(010).

Here, using different theoretical methods based on Density Functional Theory, we discuss possible structures for the (010) surface of $Al_{45}Cr_7$. Electronic structure calculations, including band structure calculations, projected density of states and projected crystal orbital Hamilton populations, help to characterize the bonding network in the bulk compound. The interplay between the three-dimensional bulk atomic arrangements and the two-dimensional surface is further investigated, based on surface energy calculations.

The more stable surface structures are found to result from a cleavage of the crystal between adjacent atomic planes, in agreement with the layered structure of the compound. The integrity of the icosahedral atomic arrangements (icosahedral clusters) found in the bulk structure, is predicted to be removed at the surface. This result is in contrast to what has been previously concluded for the (010) surface of the $Al_{13}Fe_4$ quasicrystal approximant [14,28]. More precisely, a recent investigation of $Al_{13}Fe_4$(010) using both experimental and *ab initio* computational methods indicated that the topmost surface layers correspond to incomplete puckered planes present in the bulk crystal structure, the main building block of the corrugated termination consisting of two adjacent pentagons of Al atoms, each centered by a protruding Fe atom. Differences in the bonding network of $Al_{13}Fe_4$ and $Al_{45}Cr_7$ are raised as possible reasons for such contrasted behavior.

Models and Methods

Computational details

Electronic structure calculations were performed using the plane wave Vienna *ab initio* simulation package (VASP) [29-32]. We applied the spin polarized projector-augmented wave method [33,34], within the generalized gradient approximation (GGA-PBE) [35,36], to describe the interactions between the valence electrons and the ionic core. We considered atomic valences to be $3s^23p^1$ (Al) and $3p^64s^13d^5$ (Cr). Total energies were minimized until the energy differences were less than 10^{-6} eV between two electronic cycles during the structural optimizations. Atomic

structures were relaxed until the Hellmann-Feynman forces were as low as 0.02 eV/Å. They were plotted using the VESTA software [37].

Bulk calculations were performed using a 450 eV cut-off energy and a Γ-centered 5x13x9 *k*-point grid. We used the projected Crystal Orbital Hamilton Population (pCOHP) approach, implemented in the LOBSTER code [38-41], to analyze the chemical bonding. This method re-extracts Hamilton-weighted populations from plane-wave electronic structure calculations to develop a tool analogous to the crystal orbital Hamilton population method [39]. The electrons wave functions were projected onto the atomic local basis used for the DFT calculations ($3s^2 3p^1$ for Al, $3p^6 4s^1 3d^5$ for Cr). The charge spilling, i.e. electrons which cannot be projected onto the local basis, was found to be 1.71 %. Possible charge transfers were probed through Bader charge analysis on a charge density grid [42-45].

Surface energy calculations

The approach used to compute surface energies in this work is the typical symmetric slab model, wherein a supercell of the $Al_{45}Cr_7$ crystal oriented to expose its (010) surface is generated (*p*-layer thick symmetric slabs with $p \geq 10$), and atoms are removed from a portion of the supercell to create a vacuum (void thickness ≈ 15 Å). This set-up for surface modeling leads to surface energies converged within 10 mJ/m^2 (Fig. 1).

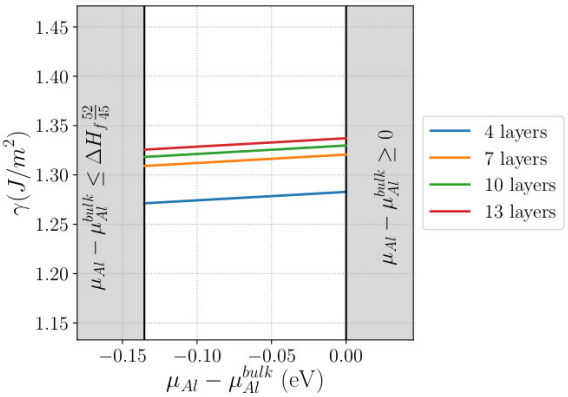

Figure 1. Surface energy as a function of the slab thickness, calculated with the P^{flat} model (see section Results and Discussion).

In the case of an elemental metal, surface energies of (hkl) orientations calculated within the symmetric slab model are given by

$$\gamma^{\sigma}_{(hkl)} = \frac{E^{\sigma}_{slab(hkl)} - n_{slab} E_{bulk(hlk)}}{2 A_{slab(hkl)}}$$

where $E_{slab(hkl)}$ is the total energy of the slab model with termination σ, $E_{bulk(hkl)}$ is the energy per atom of the bulk built using an oriented unit cell where the **a** and **b** lattice vectors are parallel to the (hkl) plane, $n_{slab(hkl)}$ is the total number of atoms in the slab structure, $A_{slab(hkl)}$ is the surface area of the slab structure, and the factor of 2 in the denominator accounts for the two surfaces in the slab model.

In the case of compounds, the stoichiometry of the slab generally differs from the one of the bulk. The surface energy is then determined as a function of the chemical potentials (μ_i) and number of atoms (N_i) of type *i* in the slab [46]:

$$\gamma^{\sigma}_{(hkl)} = \frac{E^{\sigma}_{slab(hkl)}(N_i) - \Sigma N_i \mu_i}{2 A_{slab(hkl)}}$$

In the previous equation, the numerator can be understood as the difference between the total energy of the slab and the energy of the corresponding "bulk" with the same stoichiometry.

For condensed states, the chemical potential of species *i* (μ_i), defined as the derivative of the Gibbs free enthalpy G for a given phase with respect to the number of particles *i* and fixed numbers of other particles $\{N_j\}$ apart from N_i, that is $\mu_i = \left(\frac{\partial G}{\partial N_i}\right)_{P,T,N_j}$, can be taken as the total energy per atom calculated at T = 0 K. In the case of elemental metals, the chemical potentials are then calculated as the cohesive energies, that is, $E_{coh} = \frac{E_{bulk} - E_{atom}}{N_{bulk}}$ where E_{bulk} and E_{atom} are the total energies of the bulk and an isolated atom of the same crystal, respectively, and N_{bulk} is the number of atoms in the crystal cell. In the case of intermetallic compounds, the chemical potentials are given by the Gibbs phase rule (equilibrium conditions).

Our values for the Al and Cr chemical potentials (μ_{Al}^{bulk}, μ_{Cr}^{bulk}) in fcc Al and bcc Cr, respectively, are in good agreement with experimental data as well with other DFT calculations (Tab. 1). The chemical potentials of Al (μ_{Al}) and Cr (μ_{Cr}) at the surface of the ordered Al-Cr alloy with bulk composition $Al_{45}Cr_7$ are given by $52\,\mu^{bulk}_{Al_{45}Cr_7} = 45\,\mu_{Al} + 7\,\mu_{Cr}$. They are constrained in a range, i.e. $\frac{52}{45}\Delta H_f \leq \mu_{Al} - \mu^{bulk}_{Al} \leq 0$ for Al, where ΔH_f is the formation enthalpy of the complex phase: $\Delta H_f = \frac{E^{Al_{45}Cr_7}_{bulk} - 90\,E^{Al}_{bulk} - 14\,E^{Cr}_{bulk}}{104}$, where $E^{Al_{45}Cr_7}_{bulk}$ is the total energy of bulk $Al_{45}Cr_7$ and E^{Al}_{bulk} and E^{Cr}_{bulk} are the total energies per atom of the elemental Al and Cr metals, respectively. We calculated ΔH_f = −0.117 eV/at., in good agreement with other experimental or theoretical values (Tab. 1) [47, 48, 20].

Table 1. Cohesive energies for fcc Al and bcc Cr. Formation enthalpy of $Al_{45}Cr_7$.

	E_{coh} (eV)	Ref.
Al fcc	-3.48	our work
	-3.55	calc. [49]
	-3.39	exp. [50]
Cr bcc	-4.09	our work
	-3.80	calc. [51]
	-4.00	calc. [52]
	-4.15	calc. [53]
	-4.10	exp. [50,54]
	ΔH_f (eV/at.)	Ref.
$Al_{45}Cr_7$	-0.117	our work
	-0.085	calc. [47]
	-0.139	Exp. [48,20]

Results and Discussion

Bulk $Al_{45}Cr_7$

Bulk $Al_{45}Cr_7$ crystallizes in the *C2/m* space group, with a monoclinic crystal cell containing 104 atoms (90 Al + 14 Cr). The lattice parameters are *a* = 2.0650(2) nm, *b* = 0.75978(8) nm, *c* = 1.0967(1) nm and β = 107.308(2)° [18,55], in good agreement with those deduced from DFT calculations (a = 2.059 nm, b = 0.756 nm, c = 1.092 nm and β = 107.35°) and used in this study.

The $Al_{45}Cr_7$ bulk has a layered structure described by the stacking of two types of layers in the [010] direction : flat layers (L^{flat}) made of 17 Al and 3 Cr atoms per surface cell, and puckered layers (L^{corr}), having 28 Al and 4 Cr atoms per surface cell. The stacking sequence is $L_1^{flat} L_1^{corr} L_2^{flat} L_2^{corr}$ and the interlayer distance is approximately 2 Å. Symmetries include a mirror plane, coincident with a L^{flat} plane, i.e. perpendicular to [010], and a 2-fold axis, along [010]. An alternative description of bulk $Al_{45}Cr_7$ is based on distorted icosahedral building blocks which form chains in the monoclinic direction ([010] direction). Three types of such building blocks are found in the bulk structure, as shown in Fig. 2, centered at three different Wyckoff positions (2a, 4f and 8i). They are equatorially truncated by L^{flat} planes (blue and green icosahedral clusters) or by L^{corr} planes (red clusters).

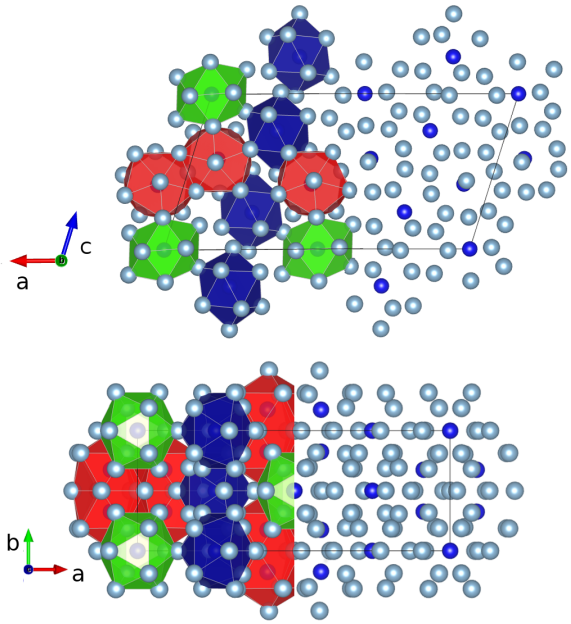

Figure 2. $Al_{45}Cr_7$ bulk structure (Atomic color code: Al = light blue, Cr = dark blue). The three Cr atom types are surrounded by icosahedral polyhedra (Cr1(2a) = green ; Cr2(4f) = blue; Cr3(8i) = red).

The electronic structure of $Al_{45}Cr_7$ shows a parabolic dispersion in the [-11,-4] eV region, with a main contribution from *sp*-Al states (Fig. 3). Two strong maxima are noticeable in the [-3,3] eV region, caused by localized and weakly dispersive Cr-d states. A deep pseudo-gap is found between these two maxima, at the Fermi energy, which contributes to the stability of this phase [56,57]. According to a previous study, the origin of the pseudo-gap is attributed to both a Hume-Rothery mechanism coupled with a strong sp-d hybridization [27].

Using the partitioning criteria proposed by Bader [44], we calculated an averaged electron transfer between Al (*+0.23* e) and Cr (*-1.47* e) atoms. This is consistent with the slightly larger Pauling electronegativity for Cr compared to Al. The same trend is found in the other complex Al_8Cr_5 phase (R-cell γ-brass) [58], with an equivalent electron depletion for Al atoms (Al : *+0.30* e, Cr : *-0.47* e). The shapes found for the Bader volumes around Cr atoms reflect their environment and are far from spherical (Fig. 4a).

Bonding analysis based on the COHP curves and their integrated values indicates that the majority of the bonding interactions reside between the Al-Al and Al-Cr pairs, whereas the homoatomic Cr-Cr interactions play minor roles and exhibit a small antibonding character (Fig. 4, ICOHP = -0.79 eV/bond, r_{Cr-Cr} = 2.68 Å). Indeed, the ICOHP values, averaged over Al-Al and Al-Cr distances (2.45 Å < r < 2.81 Å) are calculated to be -1.81 eV/bond and -1.19 eV/bond, respectively. The strongest ICOHPs are -2.24 eV (r_{Al-Al} = 2.80 Å) and -1.60 eV (r_{Cr-Al} = 2.48 Å) for Al-Al and Al-Cr interactions, respectively. Hybridization of Al-*sp* with Cr-*d* states is maximum around -2 eV. On average, the $Al_{45}Cr_7$ structure avoid any antibonding Al-Al and Al-Cr interactions, which contributes to the stability of the compound (Fig. 4b).

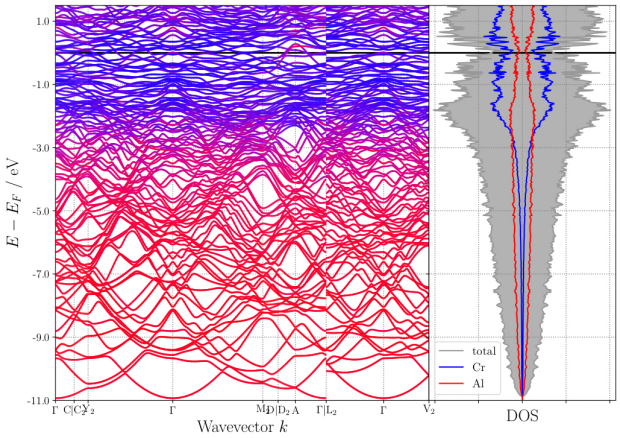

Figure. 3. Band structure and projected density of states for bulk $Al_{45}Cr_7$. States are projected over Al (red) and Cr (blue) atoms.

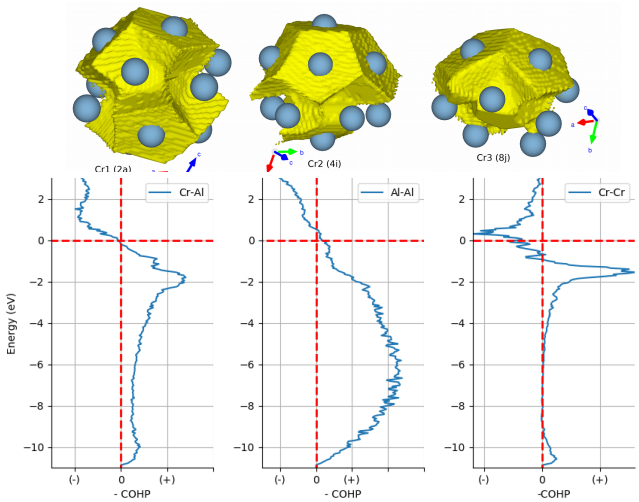

Figure 4. : (top) Shape of the Bader volumes around the three Cr atom types. Al atoms are represented in light blue. (bottom) Averaged COHPs for Al-Al, Al-Cr and Cr-Cr interactions (r < 3.2 Å).

$Al_{45}Cr_7$(010) : surface energy calculations

We started our work with a systematic screening of surface orientations, using the approach proposed by Ref. [59] based on the assumption that low-energy surfaces are planes with high atomic density. This step leads to the conclusion that triplets of atoms sample the (010) surface the most frequently, at 41.3 % of the time, followed by (001) and (100) with 28.4 % and 20.2 % each, and then (20$\bar{1}$), (110), (310) (the corresponding screening heuristic lies between 1 % and 3 %).
We then focused on the $Al_{45}Cr_7$(010) surface structure. We started the investigation using four types of surface models built from bulk truncation (Fig. 5). Two of them are built by selecting the dense L^{flat} or L^{corr} layers as topmost layer, leading to the P^{flat} and P^{corr} models, respectively. The terminations of the two other types of models are much more corrugated. They keep the cluster substructure intact at the surface, either with the green and blue icosahedral polyhedra protruding ($P^{cluster}_{2a-4i}$ model), , or with the red ones emerging ($P^{cluster}_{8j}$ model). Additional models result from the formation of surface Cr vacancies (labeled with *vac*). We also tested the influence of surface Al vacancies : the $Q^{cluster}_{2a-4i}$ model is one of those.

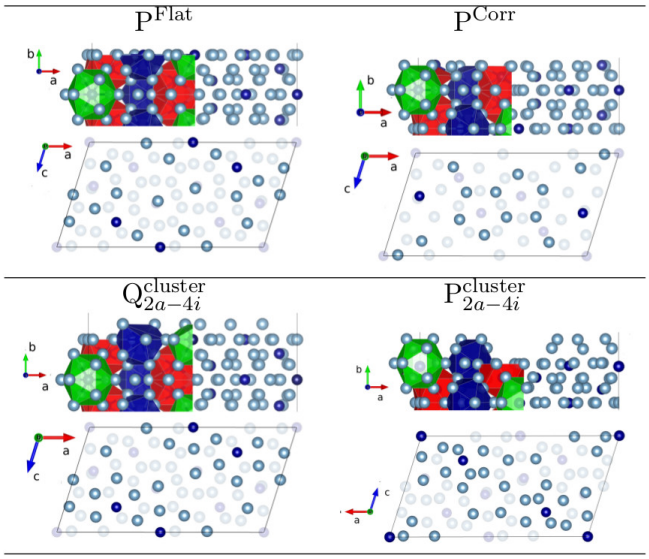

Figure 5. Surface models considered in this study (top and side views). Al = light blue, Cr = dark blue.

The surface energies of all models have been calculated. The most stable ones are shown in Fig. 6. All cluster terminated models present a high surface energy (the highest one being the one of $P^{cluster}_{8j}$) which is attributed to the open character of the surface. The *almost* cluster-based terminated model ($Q^{cluster}_{2a-4i}$), although more stable than $P^{cluster}_{8j}$ and $P^{cluster}_{2a-4i}$ presents a higher surface energy than the ones of P^{flat} and $^{vac}P^{corr}$ (Fig. 6). The addition of surface Cr vacancies ($^{vac}Q^{cluster}_{2a-4i}$) strongly destabilizes this surface model: the surface energy ranges from 1.37 J/m² ($\mu_{Al}=\mu^{bulk}_{Al}$) to 1.61 J/m² ($\mu_{Cr}=\mu^{bulk}_{Cr}$).

Models built by selecting a bulk atomic plane as termination plane are the most stable. As in the case of simple metals, the surface atomic density is a key factor for the surface stability: in the full range of chemical potentials, the P^{corr} model (32 at./surf. cell) presents a lower surface energy than the P^{flat} one (20 at./surf. cell). The presence of protruding surface Cr atoms is not likely in the Al-rich region, in relation to the higher surface energy of Cr(110) compared to Al(111) ($\gamma^{exp}_{Cr(100)}$=2.35 J/m², $\gamma^{exp}_{Al(111)}$= 1.14 J/m² [60]): surface : surface Cr vacancies lead to a decrease of the calculated surface energy, in the Al-rich region, for both P^{flat} and P^{corr} models. The previous observation is valid in the full range of chemical potentials in the case of the P^{corr} model, possibly related to the weaker bond strength of Al-Cr compared to Al-Al.

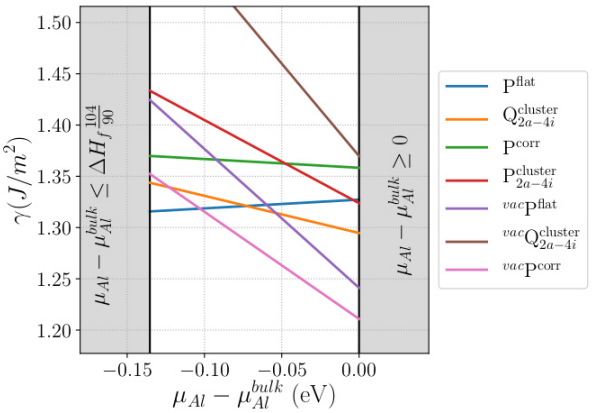

Figure 6. Surface energies of the considered models.

$Al_{45}Cr_7$(010) : surface electronic structures

STM images were simulated using the Tersoff-Hamann [61,62] approach, which provides a reliable qualitative picture of the surface topography. In this method, the surface is treated exactly, while the tip is modeled as a locally spherical potential well. The simulated images are quite different for the considered models (Fig. 7), thus demonstrating that it could be possible to discriminate them by a qualitative comparison with high-resolution experimental STM images. In most cases, the brightest contrasts are induced by the presence of protruding surface Cr atoms (P^{corr}, $Q^{cluster}_{2a-4i}$, $P^{cluster}_{2a-4i}$). The exception is the case of the P^{flat} and $^{vac}P^{flat}$ models: the simulated STM images, which look very similar, reveal large bright protrusions. The latter do most probably not arise from single surface atoms but by groups of topmost Al atoms. It seems then difficult to draw any conclusion about the nano-structured character of the surface based only on STM image observations.

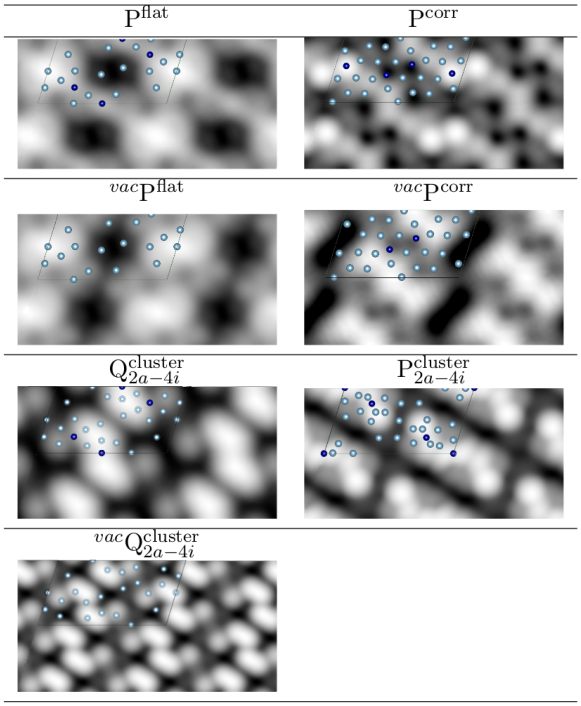

Figure 7. Simulated STM images (2.1x4.1 nm^2, V_{bias}= 1 V)

The surface electronic structure has been calculated for the $^{vac}P^{corr}$ model (Fig. 8), using a thicker slab than previously (thickness ≈ 16 Å). The contributions of *s*-states located close to the Fermi energy, are shifted at the surface, in comparison to the bulk. In addition, the presence of Cr atoms slightly below the mean position of the termination plane leads to small differences between surface and bulk contributions, especially in the *d*-states. Surface COHP have been determined, using a 12.5 Å thick slab, but no noticeable differences have been found when comparing the Al-Cr bonding environment between Cr atoms located in the subsurface layer or in the center of the slab (L^{flat} layers).

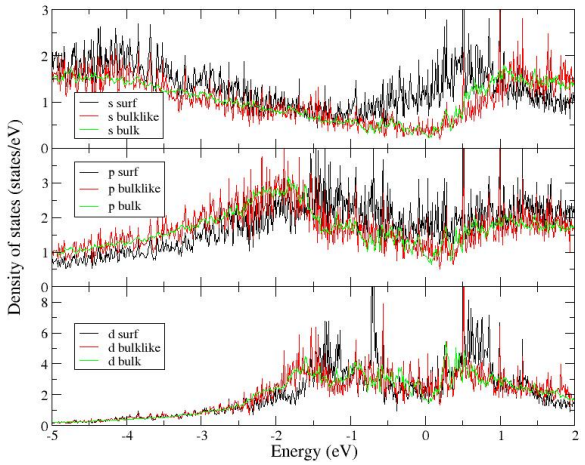

Figure 8. Contributions of *s*-, *p*- and *d*-states to the electronic structure of the most stable surface model. Color code: surface layer = black, equivalent atomic layer in the center of the slab = red, equivalent atomic layer in the bulk system = green. The agreement of the bulklike and bulk contributions illustrates that the slab is thick enough to render a bulklike behavior in the center of the slab.

$Al_{45}Cr_7$(010) versus $Al_{13}Fe_4$(010)

The surface energies of simple metals are a fraction of their cohesive energy, the proportionality constant being correlated to the number of broken bonds at the surface. The broken bond model however fails to predict the correct proportionality constant, because it neglects the variation of the bond strength with the coordination number. For example, bonds between an atom with a few neighbors are generally stronger than those between an atom with many neighbors [63,64]. In the case of intermetallics, the situation is even more complex, since additional phenomena, like charge transfer, make the chemical bond polar and asymmetric. In addition, the surface energy is influenced by the chemical potentials involved, i. e. on the experimental conditions (exact composition of the compound, surface preparation conditions, etc). The impact is all the larger on the absolute values of surface energies that the stoichiometry of the slab used to model the surface is far from that of the bulk system.

While a few structural features are shared between the two complex $Al_{13}Fe_4$ and $Al_{45}Cr_7$ compounds -- they both present a monoclinic cell, their bulk structure being described as a stacking of two types of planes -- their surface structures are quite different. In the full range of chemical potentials, the $Al_{45}Cr_7$(010) terminations with the lowest surface energies among the considered surface models, result from the selection of specific atomic planes as surface planes, possibly with Cr vacancies. The combination of surface science experiments and DFT calculations show that the $Al_{13}Fe_4$(010) surface forms at incomplete puckered planes that exist in the bulk structure [14]. These highly corrugated planes result from the preservation of the cluster building blocks at the surface, in relation to strong covalent interactions present in this compound [28].

What can be the origin of the contrasted $Al_{13}Fe_4$(010) and $Al_{45}Cr_7$(010) surfaces structures? The ratio $\frac{ICOHP(Al-Al)}{ICOHP(Al-TM)}$ of the strongest Al-Al and Al-TM bonds is very similar in $Al_{13}Fe_4$ and $Al_{45}Cr_7$: it is calculated to be 1.4. The contrasted values for the strongest Al-TM bonds in the two compounds -- $Al_{13}Fe_4$ (-ICOHP=1.83 eV/bond [28]) and $Al_{45}Cr_7$ (-ICOHP=1.60 eV/bond) -- may provide an explanation, if we assume a negligible role of the chemical potential: breaking the strong Al-Fe bonds which supports the Henley-type cluster in $Al_{13}Fe_4$ is more difficult than breaking the Al-Cr bonds supporting the clusters in $Al_{45}Cr_7$.

Conclusions

We have reported a detailed analysis of the $Al_{45}Cr_7$(010) surface, using calculations based on the Density Functional Theory. Electronic structure calculations point the presence of a deep pseudo-gap at the Fermi level, which may contribute to the stability of the compound. The COHP analysis reveals the strength of the Al-Al and Al-Cr bonds.

Several slabs were built to model the surface. Our calculations show that the (010) termination with the lowest surface energy in a wide range of chemical potentials in the Al-rich region is the one resulting from the selection of the densest atomic plane as surface plane, with Cr vacancies. The cluster terminated surface models are not identified as the most stable ones. This

conclusion is consistent with what has already been determined for Al-based quasicrystals and approximants [65], like $Al_{13}Co_4$(100) [66]. Our surface model for $Al_{45}Cr_7$(010) is however quite different from the one of $Al_{13}Fe_4$(010), a corrugated surface keeping intact the cluster substructure up to the surface, even if the two compounds share common structural features, like the monoclinic cell and the description of the bulk as a stacking of two types of planes. Further experimental work is required to assess the surface model proposed in this paper.

Acknowledgments

This work is supported by the European Integrated Center for the Development of New Metallic Alloys and Compounds. Some of us acknowledge financial support through the COMETE project (COnception in silico de Matériaux pour l'EnvironnemenT et l'Énergie) co-funded by the European Union under the program *FEDER-FSE* Lorraine et Massif des Vosges 2014-2020. High Performance Computing resources were provided by GENCI under the allocation 99642, as well as the EXPLOR center hosted by the Université de Lorraine (allocation 2017M4XXX0108).

Keywords: Quasicrystalline approximant • Surface structure • $Al_{45}Cr_7$ • DFT

[1] J. Dshemuchadse and W. Steurer. Some statistics on intermetallic compounds. Inorganic Chemistry, 54:1120-1128, 2015.
[2] T. Weber, J. Dshemuchadse, M. Kobas, M. Conrad, B. Harbrecht, and W. Steurer. Large, larger, largest ... a family of cluster-based tantalum copper aluminides with giant unit cells. I. structure solution and refinement. Acta Crystallographica Section, B65:308-317, 2009.
[3] M. Conrad, B. Harbrecht, T. Weber, D. Y. Jung, and W. Steurer. Large, larger, largest ... a family of cluster-based tantalum copper aluminides with giant unit cells. II. the cluster structure. Acta Crystallographica Section, B65:318-325, 2009.
[4] P. Chai, M. Abramchuk, and M. Shatruk. Synthesis, Crystal Structure, and Magnetic Properties of Giant Unit Cell Intermetallics $R_{117}Co_{52+\delta}Sn_{112+\gamma}$ (R = Y, La, Pr, Nd, Ho). Crystals, 6:165, 2016.
[5] J. M. Dubois. Properties and applications of quasicrystals and complex metallic alloys. Chem. Soc. Rev., 41:6760-6777, 2012.
[6] M. Armbruster, K. Kovnir, M. Friedrich, D. Teschner, G. Wowsnick, M. Hahne, P. Gille, L. Szentmiklosi, M. Feuerbacher, M. Heggen, F. Girgsdies, D. Rosenthal, R. Schlogl, and Y. Grin. $Al_{13}Fe_4$ as a low-cost alternative for palladium in heterogeneous hydrogenation. Nat. Mater., 11:690-693, 2012.
[7] M. Krajci and J. Hafner. Intermetallic compounds as selective heterogeneous catalysts : Insights from DFT. ChemCatChem, 8:34-48, 2016.
[8] J. Y. Park, D. F. Ogletree, M. Salmeron, R. A. Ribeiro, P. C. Canfield, C. J. Jenks, and P. A. Thiel. High frictional anisotropy of periodic and aperiodic directions on a quasicrystal surface. Science, 309:1354, 2005.
[9] M. A. Van Hove, R.J. Koestner, P. C. Stair, J. P. Biberian, L. L. Kesmodel, I. Bartos, and G. A. Somorjai. The surface reconstructions of the (100) crystal faces of iridium, platinum and gold: I. experimental observations and possible structural models. Surf. Sci., 103:189, 1981.
[10] G.A. Somorjai and M.A. Van Hove. Adsorbate-induced restructuring of surfaces. Prog. Surf. Sci., 30:201-211;231, 1989.
[11] M. Gierer, M.A. Van Hove, A.I. Goldman, Z. Shen, S.-L. Chang, C.J. Jenks, C.-M. Zhang, and P.A. Thiel. Structural analysis of the five-fold symmetric surface of the $Al_{70}Pd_{21}Mn_9$ quasicrystal by low energy electron diffraction. Phys. Rev. Lett., 78:467, 1997.
[12] Z. Papadopolos, G. Kasner, J. Ledieu, E. J. Cox, N. V. Richardson, Q. Chen, R. D. Diehl, T. A. Lograsso, A. R. Ross, and R. Mc-Grath. Bulk termination of the quasicrystalline fivefold surface of $Al_{70}Pd_{21}Mn_9$. Phys. Rev. B, 88:184207, 2002.
[13] H.R. Sharma, V. Fournee, M. Shimoda, A.R. Ross, T.A. Lograsso, A.P. Tsai, and A. Yamamoto. Structure of the fivefold surface of the icosahedral Al-Cu-Fe quasicrystal: Experimental evidence of bulk truncations at larger interlayer spacings. Phys. Rev. Lett., 93:165502, 2004.
[14] J. Ledieu, E. Gaudry, L. N. Serkovic Loli, S. Alarcon Villaseca, M.-C. de Weerd, M. Hahne, P. Gille, Y. Grin, J.-M. Dubois, and V. Fournée. Structural investigation of the (010) surface of the $Al_{13}Fe_4$ catalyst. Phys. Rev. Lett., 110:076102, 2013.
[15] K. Anand, H. D. Nguyen, M. Baitinger, C. Allio, C. Krellner, Yu. Grin, J. Ledieu, V. Fournée, and É. Gaudry. $Ba_8Au_{5.25}Ge_{40.75}$(110): A Nano-Caged Surface Electronically Controlled by Barium and Gold Adatoms. J. Phys. Chem. C, 122:29298-29306, 2018.
[16] K. Anand, C. Allio, C. Krellner, H. D. Nguyen, M. Baitinger, Y. Grin, J. Ledieu, V. Fournée, and É. Gaudry. Charge balance controls the (100) surface structure of the $Ba_8Au_{5.25}Ge_{40.75}$ clathrate. J. Phys. Chem. C, 122:2215-2220, 2018.
[17] F. Abdel-Hamid, M.-C. de Weerd, J. Ledieu, . Gaudry, and V. Fournée. Investigation of the (100) Surface of the $Ce_3Pd_{20}Si_6$ Intermetallic Cage Compound. J. Phys. Chem. C, 123:12355-12366, 2019.
[18] M. J. Cooper. The structure of the intermetallic phase θ(Cr-Al). Acta Crystallographica, 13(3):257-263, 1960.
[19] M. Audier, M. Durand-Charre, E. Laclau, and H. Klein. Phase equilibria in the Al-Cr system. Journal of Alloys and Compounds, 220:225-230, 1995.
[20] K. Mahdouk and J.-C. Gachon. Thermodynamic Investigation of the Aluminum-Chromium System. Journal of Phase Equilibria, 21:157-166, 2000.
[21] B.B. Cao and K.H. Kuo. Crystal structure of the monoclinic η-$Al_{11}Cr_2$. Journal of Alloys and Compounds, 458:238-247, 2008.
[22] B.B. Cao. On the structure of the hexagonal μ-Al4Cr and its relation to the monoclinic η-$Al_{11}Cr_2$. Journal of Alloys and Compounds, 698:605-610, 2017.
[23] X. Z. Li, K. Sugiyama, K. Hiraga, A. Sato, A. Yamamoto, H. X. Sui, and K. H. Kuo. Crystal structure of orthorhombic ε-Al_4Cr. Zeitschrift fur Kristallographie, 212:628-633, 1997.
[24] F. A. Crossley and L. F. Mondolfo. Mechanism of Grain Refinement: in Aluminum Alloys. Journal of metals, 3:1143-1148, 1951.
[25] G. Kurtuldu, Ph. Jarry, and M. Rappaz. Influence of Cr on the Nucleation of Primary Al and Formation of Twinned Dendrites in Al-Zn-Cr Alloys: Can Icosahedral Solid Clusters Play a Role? Acta Mater., 61:7098, 2013.
[26] M. Rappaz and G. Kurtuldu. Quasicrystal-enhanced nucleation during the solidification of fcc metallic alloys: A tentative thermodynamic approach. J. Phase Equilib. Diffus., 37:2-3, 2016.
[27] P. Boulet, M.-C. deWeerd, E. Gaudry, J. Ledieu, and V. Fournee. Single crystal growth, crystal structure and surface characterisation of the binary phase $Al_{45}Cr_7$. IOP Conf. Ser., Mater. Sci. Eng., 2020.
[28] Ph. Scheid, C. Chatelier, J. Ledieu, V. Fournee, and E. Gaudry. Bonding Network and Stability of Clusters: The Case Study of the $Al_{13}TM_4$ Pseudo-10fold Surfaces. Acta Crystallogr. A, 75:314-324, 2019.
[29] G. Kresse and J. Hafner. Ab initio molecular dynamics for liquid metals. Phys. Rev. B, 47:558-561, 1993.
[30] G. Kresse and J. Hafner. Ab initio molecular-dynamics simulation of the liquid-metal-amorphous-semiconductor transition in germanium. Phys. Rev. B, 49:14251-14269, 1994.
[31] G. Kresse and J. Furthmuller. Efficient iterative schemes for ab initio total-energy calculations using a plane-wave basis set. Phys. Rev. B, 54:11169-11186, 1996.
[32] G. Kresse and J. Furthmuller. Efficiency of ab-initio total energy calculations for metals and semiconductors using a plane wave basis set. Comput. Mater. Sci., 6:15-50, 1996.
[33] P. E. Blochl. Projector augmented-wave method. Phys. Rev. B, 50:17953-17979, 1994.
[34] G. Kresse and D. Joubert. From ultrasoft pseudopotentials to the projector augmented-wave method. Phys. Rev. B, 59:1758-1775, 1999.
[35] J. P. Perdew, K. Burke, and M. Ernzerhof. Generalized gradient approximation made simple. Phys. Rev. Lett., 77:3865, 1996.
[36] J. P. Perdew, K. Burke, and M. Ernzerhof. Erratum: Generalized gradient approximation made simple. Phys. Rev. Lett., 78:1396, 1997.
[37] K. Momma and F. Izumi. VESTA 3 for three-dimensional visualization of crystal, volumetric and morphology data. J. Appl. Crystallogr., 44:1272-1276, 2011.
[38] R. Dronskowski and P. E. Blochl. The original COHP definition. J. Phys. Chem., 97:8617-8624, 1993.
[39] V. L. Deringer, A. L. Tchougreff, and R. Dronskowski. Crystal orbital hamilton population (COHP) analysis as projected from plane-wave basis sets. J.Phys.Chem. A, 115:5461-5466, 2011.
[40] S. Maintz, V. L. Deringer, A. L. Tchougreeff, and R. Dronskowski. The mathematical apparatus and the framework on which LOBSTER is built. J. Comput. Chem., 34:2557-2567, 2013.
[41] S. Maintz, V. L. Deringer, A. L. Tchougreeff, and R. Dronskowski. LOBSTER: A tool to extract chemical bonding from plane-wave based DFT. J. Comput. Chem., 37:1030-1035, 2016.
[42] W. Tang, E. Sanville, and G. Henkelman. A grid-based Bader analysis algorithm without lattice bias. Journal of Physics : Condensed Matter, 21:084204, 2009.
[43] E. Sanville, S. D. Kenny, R. Smith, and G. Henkelman. An improved grid-based algorithm for Bader charge allocation. J. Comp. Chem., 28:899-908, 2007.
[44] G. Henkelman, A. Arnaldsson, and H. Jonsson. A fast and robust algorithm for bader decomposition of charge density. Comput. Mater. Sci., 36:254-360, 2006.

[45] M. Yu and D. R. Trinkle. Accurate and efficient algorithm for Bader charge integration. J. Chem. Phys., 134:064111, 2011.
[46] F. Bechstedt. Principles of surface physics. Springer, Berlin, 2003.
[47] M. Mihalkovic and M. Widom. http://alloy.phys.phys.cmu.edu.
[48] O. Kubaschewski and G. Heymer. Heat of formation of transition metal aluminides. Trans. Faraday Soc., 56:473-478, 1960.
[49] F. Chiter, V. B. Nguyen, N. Tarrat, M. Benoit, H. Tang, and C. Lacaze-Dufaure. Effect of van der Waals corrections on DFT-computed metallic surface properties. Mater. Res. Express, 3:046501, 2016.
[50] C. Kittel. Introduction to Solid State Physics. John Wiley & Sons, USA, 7 edition, 1996.
[51] P. H. T. Philipsen and E. J. Baerends. Cohesive energy of 3d transition metals: Density functional theory atomic and bulk calculations. Phys. Rev. B, 54:5326-5333, 1996.
[52] P. Janthon, S. Luo, S. M. Kozlov, Francesc Vines, J. Limtrakul, D. G. Truhlar, and F. Illas. Bulk properties of transition metals: A challenge for the design of universal density functionals. J. Chem. Theory
Comput., 10:3832-3839, 2014.
[53] R. Hafner, D. Spisak, R. Lorenz, and J. Hafner. Magnetic ground state of Cr in density-functional theory. Phys. Rev. B, 65:184432, 2002.
[54] V. L. Moruzzi and P. M. Marcus. Antiferromagnetism in 3d transition metals. Phys. Rev. B, 42:8361, 1990.
[55] Z.B.He, B.S. Zou, and K.H. Kuo. The monoclinic $Al_{45}Cr_7$ revisited. Journal of Alloys and Compounds, 417:L4-L8, 2006.
[56] Uichiro Mizutani and Hirokazu Sato. The Physics of the Hume-Rothery Electron Concentration Rule. Crystals, 7:9, 2017.
[57] Guy Trambly de Laissardière, D. Nguyen Manh, and D. Mayou. Electronic structure of complex Hume-Rothery phases and quasicrystals in transition metal aluminides. Progress in Materials Science, 50:679-788, 2005.
[58] Uichiro Mizutani. Hume-Rothery Rules for Structurally Complex Alloy Phases. Taylor Francis US, 2010.
[59] Wenhao Sun and Gerbrand Ceder. A topological screening heuristic for low-energy, high-index surfaces. Surface Science, 669:50-56, 2018.
[60] W.R. Tyson and W.A. Miller. Surface free energies of solid metals: Estimation from liquid surface tension measurements. Surf. Sci., 62:267, 1977.
[61] J. Tersoff and D. R. Hamann. Theory and application for the scanning tunneling microscope. Phys. Rev. Lett., 50:1998-2001, 1983.
[62] J. Tersoff and D. R. Hamann. Theory of the scanning tunneling microscope. Phys. Rev. B, 31:805-813, 1985.
[63] M. Methfessel, D. Hennig, and M. Scheffler. Calculated surface energies of the 4d transition metals: A study of bond-cutting models. Appl. Phys. A, 55:442, 1992.
[64] V. Heine, I.J. Robertson, and M.C. Payne. Many-atom interactions in solids. Philos. Trans. R. Soc. A, 334:393, 1991.
[65] Julian Ledieu and Vincent Fournée. Surfaces of quasicrystals. C. R. Physique, 15:48-57, 2014.
[66] E. Gaudry, C. Chatelier, G. McGuirk, L. Serkovic Loli, M.-C. De-Weerd, J. Ledieu, V. Fournée, R. Felici, J. Drnec, G. Beutier, and M. de Boissieu. Structure of the $Al_{13}Co_4$(100) surface: Combination of surface x-ray diffraction and ab initio calculations. Phys. Rev. B, 94:165406, 2016.

Entry for the Table of Contents (Please choose one layout)

Layout 1:

FULL PAPER

Text for Table of Contents

*Author(s), Corresponding Author(s)**

Page No. – Page No.

Title

((Insert TOC Graphic here: max. width: 5.5 cm; max. height: 5.0 cm))

Layout 2:

FULL PAPER

*Author(s), Corresponding Author(s)**

((Insert TOC Graphic here; max. width: 11.5 cm; max. height: 2.5 cm))

Page No. – Page No.

Title

Text for Table of Contents

Additional Author information for the electronic version of the article.

Emilie Gaudry: 0000-0001-6546-8323